

CONCEPTUAL DESIGN OF BALLOON DOUBLE SPOKE RESONATOR*

Z. Yao†, R. E. Laxdal, TRIUMF, Vancouver, Canada

Abstract

The balloon variant of the spoke resonator was proposed to eliminate the intensive multipacting (MP) barriers around the operating field level by modifying the local electro-magnetic (EM) fields. TRIUMF has previously reported the prototyping of a 325MHz $\beta=0.3$ single spoke resonator (SSR) that demonstrated the principle of the balloon concept. To extend the benefits of the balloon variant to multi-spoke resonators, this paper will report a conceptual design of a 325MHz $\beta=0.5$ balloon double spoke resonator (DSR). The consequences from the balloon SSR design, such as the relations between EM field distributions and the field levels of the MP barriers, were applied to the DSR design. Other particular geometry features were also added due to the characters of DSRs. The simulated MP barriers were significantly squeezed to the lower field level compared to a conventional DSR design. Simulation results and conceptual design will be reported.

INTRODUCTION

Spoke resonators have been widely proposed for proton accelerators, such as ESS [1], PIP-II [2], CADS [3], CSNS [4], heavy ion accelerators like RISP [5], and compact electron accelerators [6]. The modern designs have demonstrated the promising cavity performance around the world. But as a companion, the intensive and broader MP barriers, which could extend to the operating regime of the accelerating gradient, were brought to the community's attention. Some cavities requiring hours to days RF conditioning to overcome MP barriers have been reported for both SSR and multiple spoke resonators [7, 8].

The balloon variant of spoke resonator was proposed to eliminate MP barriers around the operating field by modifying the local EM fields [9]. TRIUMF has reported the prototyping of a 325MHz $\beta=0.3$ SSR. It demonstrated that the balloon SSR constricts MP barriers well below the operating accelerating gradient and the required RF conditioning time can be reduced to minutes after in-situ low temperature baking [10]. The proven performance of the balloon concept encouraged the community to further investigate this new variant of SSR.

To augment the benefits of the balloon variant to multi-spoke resonators, this paper will report the conceptual design of the balloon DSR. The discussion starts with the conventional cavity geometry to analyze the characteristics of MP in DSR. Then the consequences from the balloon SSR are applied to the DSR design. As the geometry and the surface field distribution of DSR are more complicated, further geometry optimization is required to squeeze MP barriers to the lower gradient regime.

BASELINE

To study the balloon variant of DSR, a conventional DSR model is built as the baseline with the same resonant frequency and geometrical beta. The cavity geometry of the baseline model is optimized to obtain comparable RF parameters with existing designs. The MP barriers of DSR are characterized in the baseline. Both RF and MP are simulated with CST Studio Suite [11].

RF Optimization

To adapt the proposed proton or heavy ion accelerators, this study chooses the resonant frequency at 325 MHz and the geometrical beta of 0.5. The diameter of the beam tubes is 50 mm. The baseline model consists of a cylindrical cavity body and re-entrant end shells. The racetrack profile and transverse orientation are selected for both the spoke aperture region and spoke base to achieve lower peak surface fields and a higher shunt impedance [12]. The dimensions of the spokes and the end shells are optimized for RF parameters. The spoke positions along the beam axis are adjusted to maintain the geometrical beta. The resonant frequency is adjusted by the cavity diameter. Following the standard geometry optimization procedure, the baseline model is obtained as shown in Fig. 1 and the RF parameters are listed in Table 1 (1st column).

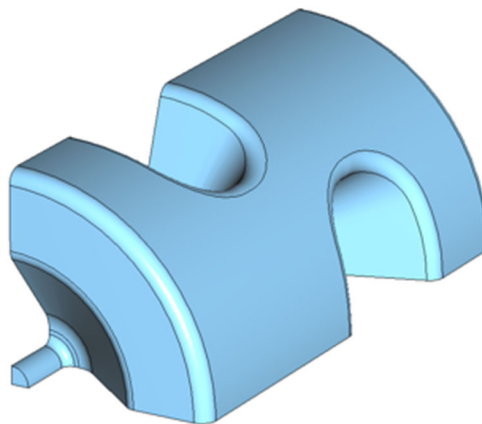


Figure 1: A quarter model of the baseline DSR model.

Multipacting

A niobium shell is added to the outer surface of the vacuum model. The shell material is defined as the 300 degC baked niobium, whose secondary electron yield (SEY) has the peak value of 1.49 at the impact energy of 300 eV. A uniform distributed particle source is defined in the simulation volume. The initial electrons are released equally every 30 degrees in the first RF period. The secondary electron counts and trajectories are recorded. The growth rate is defined as the power of the exponential increase of the secondary electrons. It represents a MP barrier when it is

* Work supported by the National Research Council Canada.

† zyyao@triumf.ca

positive. The MP barriers of the baseline model are broad, from 0.5 MV/m to above 18 MV/m, shown in Fig. 2. The 1st order barrier and the higher order barriers are separated with colors in the growth rate diagram.

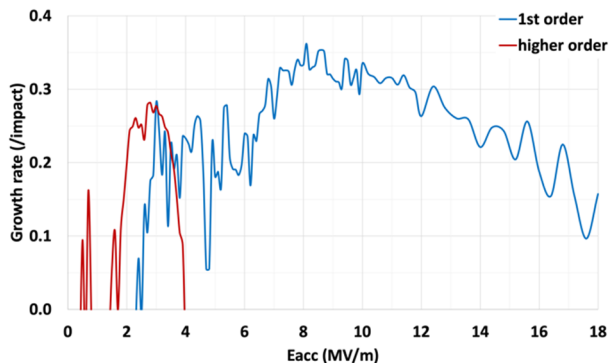


Figure 2: The growth rate (/impact) of MP barriers of the baseline model.

The trajectories of the secondary electrons of the 1st order barriers are shown in Fig. 4, while those of the higher order barriers are shown in Fig. 3. The displayed electrons in both figures are the mixed results at several accelerating gradients. It gives the overview of the MP locations on the cavity surface. In addition, the surface electric field distribution in dB scale is shown in Fig. 5. The Red color represents the peak surface field, while the Blue color is the null electric field line. The full color range is 80 dB.



Figure 3: The secondary electron trajectories of the 2nd and higher order MP barriers. The displayed results are combined data from 0.5 MV/m to 2.8 MV/m.

The 2nd order and higher orders MP barriers exist from 0.5 MV/m to 3.9 MV/m on the accelerating gradient. The trajectories around the inner side of the spoke roots in Fig. 3 represent the barriers between 0.5 MV/m and 0.7 MV/m. The secondary electrons extending from the outer side of spoke roots to the end walls represent the barriers between 1.5 MV/m to 3.9 MV/m. The surface areas of these barriers include the electric fields from -30 dB to -40 dB compared to the peak.

The 1st order MP has a much broader barrier than the higher orders', from 2.4 MV/m to above 18 MV/m. The trajectories of this barrier in Fig. 4 locate along the null

electric field line in Fig. 5, where the electric fields have the opposite directions on both sides. The magnitude of the local magnetic field along the null electric field line varies over 8 dB in the baseline model, which causes the wide barrier on accelerating gradient. The details are discussed in the later section.

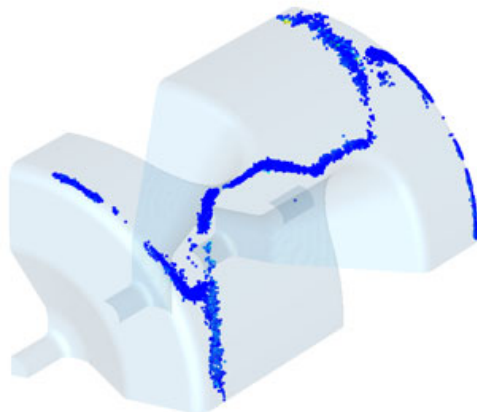


Figure 4: The secondary electron trajectories of the 1st order MP barrier. The displayed results are combined data from 3 MV/m to 9 MV/m. The trajectories on the bottom-left and top-right are excluded, which are the coincided 2nd order barriers at lower field levels.

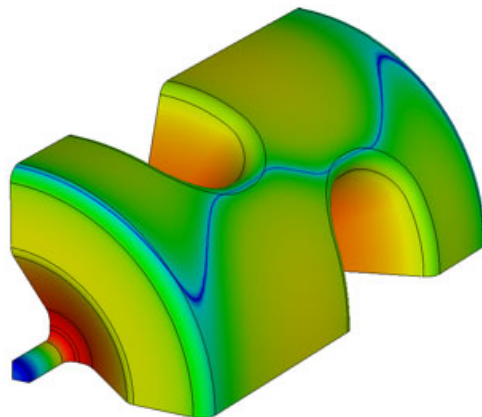


Figure 5: The surface electric field distribution shown in dB. The color range from Red to Blue is 80dB.

BALLOON

The balloon variant of SSR was previously proposed to eliminate the MP barriers around the operating field level. As the gradient of the barriers has relation with the local EM fields, the MP barriers can be optimized on the gradient by changing the local fields via modifying the cavity geometry. Furthermore, in SSR, the locations of the 1st order barrier and the higher order barriers are well separated on the cavity surface. The two critical areas for the MP optimization are identified, the spoke roots and the edge connecting the end walls to the cavity spool. Decreasing the fillet radius of the spoke roots squeezes the 1st order barrier to the lower field level, while increasing the fillet radius of

Content from this work may be used under the terms of the CC BY 4.0 licence (© 2022). Any distribution of this work must maintain attribution to the author(s), title of the work, publisher, and DOI

the latter one has the same effect on the higher order barriers.

Comparing DSR to SSR, the MP barriers existing between the outer side of the spokes and the end walls have the same behaviors. The balloon concept from SSR works in principle to suppress these barriers for DSR. The central area between the two spokes does not exist in SSR. The barriers in this area need additional consideration if they are critical. In this section, the balloon concept from SSR is applied to DSR first, then the field uniformity is discussed to further suppress MP.

Balloon Model

The initial balloon DSR model is modified from the baseline model. The fillet radius of the spoke roots is reduced to 5 mm, and the fillet of the end walls is changed to an elliptical curved face extending to the mid-plane of the closer spoke, as shown in Fig. 6.

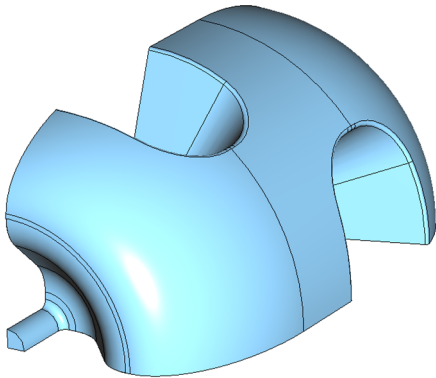


Figure 6: A quarter model of the initial balloon model.

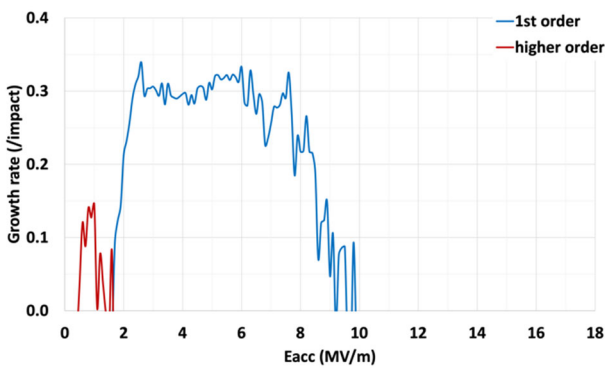


Figure 7: The growth rate (/impact) of MP barriers of the initial balloon model.

The growth rate diagram of this model is shown in Fig. 7. The effects of applying the balloon concept to DSR are obvious. The higher order barriers between the spoke and the end wall are squeezed to the gradient range from 0.5 MV/m to 1.6 MV/m and overlap the higher order barriers between both spokes. The 1st order barrier is moved to lower field level as well, between 1.7 MV/m and 9.8

MV/m. But this barrier is still broad, and the higher gradient end extends to the common operating gradient of the spoke resonators around 8 to 9 MV/m.

Field Uniformity

To further optimize the 1st order barrier to the lower field level and keep it away from the operating gradient, the magnetic field values along the null electric field line (seen in Fig. 8) are considered. Comparing to Fig. 5, the null field line in the end section is closer to the spoke root, where there are higher local magnetic fields.

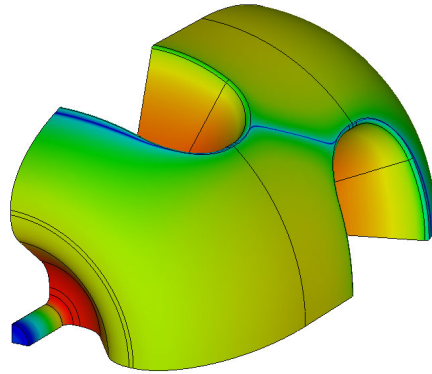


Figure 8: The surface electric field distribution shown in dB. The color range from Red to Blue is 80dB.

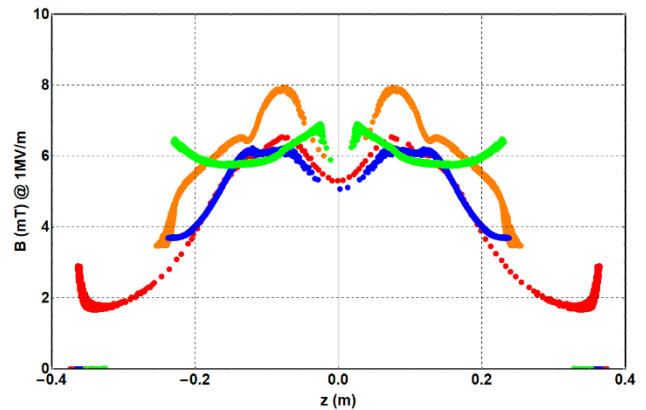


Figure 9: The magnetic field profile along the null electric field line at an accelerating gradient of 1 MV/m. The abscissa is the coordinate along the beam axis. Red – the baseline model, Orange – the initial balloon model, Green – the balloon model optimized for MP, and Blue – the balloon model optimized for RF.

To quantify the comparison, the local magnetic field profile along the null electric field line of the baseline model is plotted in Fig. 9 in Red color and that of the initial balloon model is plotted in Orange color. The magnitude of the magnetic field is normalized to the accelerating gradient at 1 MV/m. The higher minimal magnetic field (Orange vs. Red) brings the higher gradient end of the barrier from over 18 MV/m to below 10 MV/m, and the higher maximal magnetic field (Orange vs. Red) pushes the lower gradient edge from 2.4 MV/m to 1.7 MV/m. The gradient of the MP

barrier is positively correlated to the reciprocal of the magnitude of the local magnetic field. As a consequence, a constant magnitude of the magnetic field along the null electric field line can provide a narrow MP barrier on the gradient. In addition, the higher magnitude of the local field moves the barrier away from the operating gradient to the lower field level. The following geometry optimization is focused on the uniformity of the local magnetic field.

To obtain a constant magnetic field profile, the peak magnetic field in the curve can be kept in the range from 6 mT to 8 mT, and the lower ends need to be lifted. The geometry profile of the spoke roots is required to be modified to have more flux density around the outer side of spoke roots. Increasing the EM fields in the end cells also helps to lift the lower tails of the curve to the higher level. The optimized model is shown in Fig. 10. The dimension of the spoke roots is enlarged. The outer profile of the spoke roots is changed from the racetrack to the elliptical shape. The inner side is unchanged. The joint point of the ellipse and the racetrack is off the mid-plane of the spoke root. The end accelerating gaps are decreased to enhance the local RF fields, while the center gap is increased to maintain the geometrical beta.

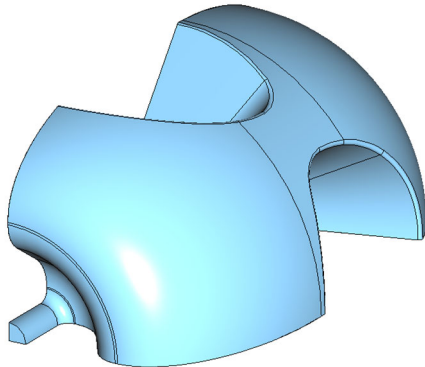


Figure 10: A quarter model of the balloon model optimized for MP considerations.

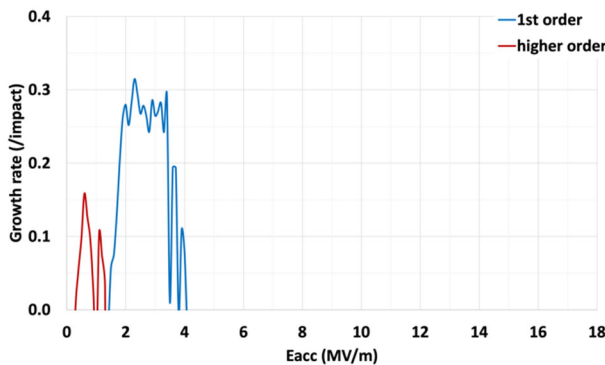


Figure 11: The growth rate (/impact) of MP barriers of the balloon model optimized for MP considerations.

The growth rate diagram of the balloon model optimized for MP consideration is shown in Fig. 11 and the local magnetic field along the null electric field line is plotted in Fig.

9 in Green color. The optimized balloon model significantly improved the field uniformity in the critical area. The magnitude range is reduced from over 4 mT to less than 1 mT compared to the initial balloon model. The effect of the constant magnetic field profile is demonstrated in the growth rate diagram. The higher gradient end of the 1st order MP barrier is pushed to 4 MV/m. It provides several MV/m margins from the operating regime.

Table 1: RF Parameter Comparison

Parameter	Unit	Base-line	Opt. MP	Opt. RF
Ep/Eacc		3.35	5.06	3.53
Bp/Eacc	mT/(MV/m)	7.69	7.73	7.05
G	Ohm	123	112	125
R/Q	Ohm	447	382	410

Further Discussion

The RF parameters of the balloon model optimized for MP considerations are listed in Table 1 compared to the baseline. As the cost of achieving the constant magnetic field, the RF parameters are degraded. Further optimizations have been studied to improve the RF parameters while constraining the MP barriers in the low gradient region. But a solution with both advantages has not been found. As a compromise, a balloon model optimized for RF parameters is obtained, shown in Fig. 12. The elliptical profile for the outer side of the spokes is maintained. The dimensions of the spoke aperture region and the spoke roots are optimized. The RF parameters are listed in Table 1 (3rd column) and the growth rate diagram is shown in Fig. 13. The model appears close to the initial balloon model. The asymmetric spoke root profile provides better uniformity of the magnetic field, shown in Fig. 9 in Blue color (vs. Orange). It gives a relatively narrower barrier for the 1st order MP, from 2 MV/m to 8.9 MV/m.

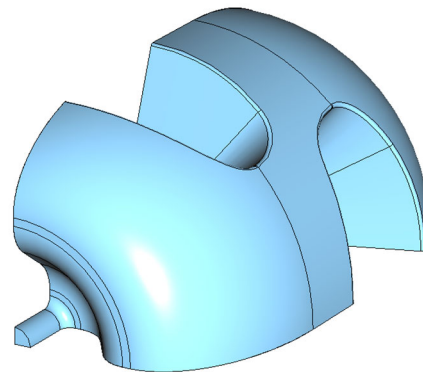


Figure 12: A quarter model of the balloon model optimized for RF parameters.

Contrasted with the conventional baseline model, both the 1st order and the higher orders MP barriers are moved to the lower field level and avoid the operating gradient

around 10 MV/m with the assumption that cavity operates at the peak electric field of 35 MV/m. Note that the balloon DSR still provides comparable RF parameters to the baseline.

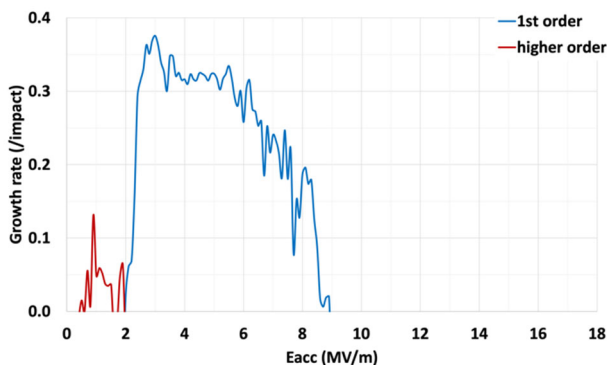


Figure 13: The growth rate (/impact) of MP barriers of the balloon model optimized for RF parameters.

CONCLUSION

Encouraged by the promising performance of the balloon SSR of the suppression effects on the MP barriers, the balloon concept is applied to DSR, and the conceptual designs of the balloon variant of DSR are reported in this paper. Compared to the balloon SSR, due to the more complicated geometry, the balloon DSR cannot be optimized on both MP and RF aspects. In our conceptual designs, one model is designed to constrain MP barriers in the lower field level with degraded RF performance, and the other is optimized to achieve high RF performance with relatively broader MP barriers. But both balloon variants of DSR conceptual design have narrower MP barriers comparing to the conventional DSR model and avoid the operating gradient region. This conceptual design demonstrates the balloon concept is compatible with DSR. Additional consideration of the magnetic field uniformity along the null electric field line is required for the more complicated structure. If proposed for an application, a hybrid variant of the balloon DSR could be optimized to meet the design specifications.

ACKNOWLEDGEMENTS

TRIUMF receives funding via a contribution through the National Research Council Canada.

REFERENCES

[1] M. Eshraqi *et al.*, “The ESS Linac”, in *Proc. 5th Int. Particle Accelerator Conf. (IPAC’14)*, Dresden, Germany, Jun. 2014, pp. 3320-3322. doi:10.18429/JACoW-IPAC2014-THPME043

[2] V. A. Lebedev, P. Derwent, and S. D. Holmes, “An 800 MeV Superconducting Linac to Support Megawatt Proton Operations at Fermilab”, in *Proc. 27th Linear Accelerator Conf. (LINAC’14)*, Geneva, Switzerland, Aug.-Sep. 2014, paper THIOA05, pp. 807-810.

[3] Z. Li *et al.*, “Physics design of an accelerator for an accelerator-driven subcritical system,” *Phy. Rev. ST Accel. Beams*, vol. 16, no. 8, p. 080101, Aug. 2013. <https://doi.org/10.1103/PhysRevSTAB.16.080101>

[4] Q. Zhou *et al.*, “Development of a superconducting radio frequency double spoke cavity for CSNS,” *Nuclear Instrum. Methods Phys. Res., Sect. A*, vol. 988, p. 164873, Feb. 2021. <https://doi.org/10.1016/j.nima.2020.164873>

[5] D. Jeon and H. J. Kim, “Status of RAON Heavy Ion Accelerator Project”, in *Proc. 27th Linear Accelerator Conf. (LINAC’14)*, Geneva, Switzerland, Aug.-Sep. 2014, paper WEIOB03, pp. 775-779.

[6] M. Sawamura *et al.*, “Development of Superconducting Spoke Cavity for Laser Compton Scattered Photon Sources”, in *Proc. 5th Int. Particle Accelerator Conf. (IPAC’14)*, Dresden, Germany, Jun. 2014, pp. 1946-1948. doi:10.18429/JACoW-IPAC2014-WEPRO005

[7] A. I. Sukhanov *et al.*, “Cold Tests of SSR1 Resonators for PXIE”, in *Proc. 16th Int. Conf. RF Superconductivity (SRF’13)*, Paris, France, Sep. 2013, paper MOP014, pp. 112-116.

[8] H. Li *et al.*, “ESS Spoke Cavity Conditioning at FREIA”, in *Proc. 8th Int. Particle Accelerator Conf. (IPAC’17)*, Copenhagen, Denmark, May 2017, pp. 1074-1076. doi:10.18429/JACoW-IPAC2017-MOPVA094

[9] Z. Yao *et al.*, “Balloon variant of single spoke resonator,” *Phys. Rev. Accel. Beams*, to be published.

[10] R. E. Laxdal and Z. Yao, “Balloon single spoke resonator - a new SSR variant for reduced multipacting,” presented at SRF’19, Dresden, Germany, June 2019, paper FRCAA2, unpublished.

[11] CST Studio Suite, <https://www.3ds.com/products-services/simulia/products/cst-studio-suite/>.

[12] C. S. Hopper *et al.*, “Superconducting spoke cavities for high-velocity applications,” *Phy. Rev. ST Accel. Beams*, vol. 16, no. 10, p. 102001, Oct. 2013. <https://doi.org/10.1103/PhysRevSTAB.16.102001>